Nonlinear Energy Harvesting

F. Cottone,* H. Vocca, and L. Gammaitoni†

NiPS Laboratory, Dipartimento di Fisica, Universitá di Perugia, and Instituto Nazionale di Fisica Nucleare, Sezione di Perugia, I-06100 Perugia, Italy

(Received 18 September 2008; published 23 February 2009)

Ambient energy harvesting has been in recent years the recurring object of a number of research efforts aimed at providing an autonomous solution to the powering of small-scale electronic mobile devices. Among the different solutions, vibration energy harvesting has played a major role due to the almost universal presence of mechanical vibrations. Here we propose a new method based on the exploitation of the dynamical features of stochastic nonlinear oscillators. Such a method is shown to outperform standard linear oscillators and to overcome some of the most severe limitations of present approaches. We demonstrate the superior performances of this method by applying it to piezoelectric energy harvesting from ambient vibration.

DOI: 10.1103/PhysRevLett.102.080601 PACS numbers: 05.40.Ca, 05.10.Ln, 05.45.−a, 84.60.−h

The efficient powering of small-scale electronic mobile devices [1–3] is still an open problem. Old-style solutions, i.e., disposable batteries, cannot always be employed due to a number of reasons, chief among others the practical impossibility of replacement once exhausted. For such reasons, a new approach based on the exploitation of energy harvested where and when available has attracted considerable attention. Specifically, vibration energy harvesting and ambient light exploitation are believed to constitute a potentially viable solution. Ambient vibrations come in a vast variety of forms from sources as diverse as wind induced movements, seismic noise, and car's motion. Present working solutions for vibration-to-electricity [4–7] conversion are based on linear, i.e., resonant, mechanical oscillators that convert kinetic energy via capacitive, inductive, or piezoelectric methods [8–10] by tuning their resonant frequency in the spectral region where most of the energy is available. However, in the vast majority of cases, the ambient vibrations have their energy distributed over a wide spectrum of frequencies, with significant predominance of low frequency components, and frequency tuning is not always possible due to geometrical or dynamical constraints [10,11].

To overcome these difficulties, we propose a different approach based on the exploitation of the properties of nonlinear (i.e., nonresonant) oscillators. Specifically, we demonstrate that a bistable oscillator, under proper operating conditions [12] can provide better performances compared to a linear oscillator in terms of the energy extracted from a generic wide spectrum vibration. In fact, a nonlinear oscillator, as the one that we discuss here, by default can present a wide spectral response (much wider than a linear or resonant one) and can be operated in such a way that its frequency response matches more closely what is available in the environment. In this regard, we point out that we are dealing here with open systems far from equilibrium, and the energy conversion mechanism is affected by both the spectral distribution and by the intensity of the vibrational energy available and is directly connected to the amplitude of the motion of the oscillating elements. Moreover, we note that the dynamical features discussed here are not limited to the sole piezoelectric energy conversion but can be applied also to other principles, e.g., capacitive and inductive.

For the sake of demonstration, we realized a toy-model oscillator made by a piezoelectric inverted pendulum (Fig. 1) where on top of the pendulum mass a small magnet (tip magnet) has been added. The effect of ground vibration force is reproduced by applying a properly designed magnetic excitation on two small magnets attached near the base of the pendulum. Under the action of the excitation, the pendulum oscillates, alternatively bending the piezoelectric beam and thus generating a measurable voltage signal. The dynamics of the inverted pendulum tip can be controlled with the introduction of an external magnet conveniently placed at a certain distance Δ and with polarities opposed to those of the tip magnet. The external magnet introduces a force dependent from Δ that opposes the elastic restoring force of the bended beam. As a result, the inverted pendulum dynamics can show two different types of behaviors as a function of the distance Δ. Specifically, when the external magnet is far away, the inverted pendulum behaves like a linear oscillator whose dynamics is resonant with a resonance frequency determined by the system parameters. This situation accounts well for the usual operating condition of traditional piezoelectric vibration-to-electric energy converters [6]. On the other hand, when Δ is small enough, two new equilibrium positions appear. The random vibration makes the pendulum swing in a more complex way with small oscillations around each of the two equilibrium positions and large excursions from one to the other. In order to quantify the energy produced by the piezoelectric oscillator, we computed the power dissipated in a purely resistive load, by

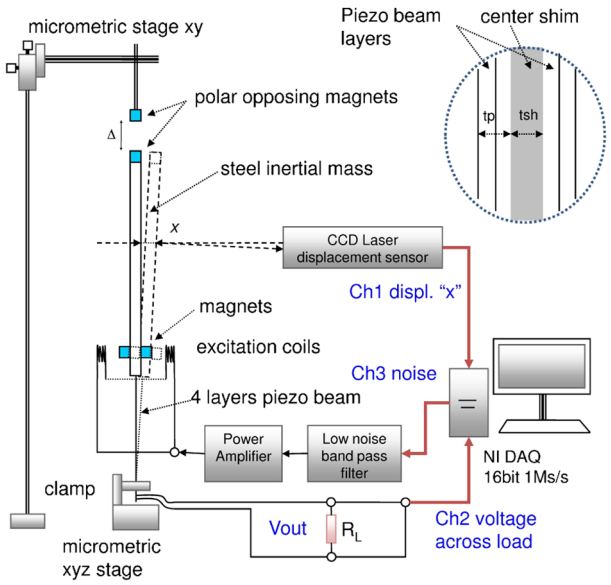

FIG. 1 (color online). Schematic of the experimental apparatus. The inverted pendulum is a four-layer piezoelectric beam made by lead zirconate titanate (PSI-5A4E) 60 mm of free length, clamped at one end. The piezoelectric beam has a width of 5 mm and a thickness of 0.86 mm. The pendulum mass is a steel cylinder 140.0 mm long and with diameter of 4.0 mm, with three magnets attached (each magnetic dipole moment is 0.051 A m^2). The inverted pendulum resonance frequency (in the linear regime) is 6.67 Hz. The displacement x is measured via an optical readout. The voltage signal from the piezo is measured through a load resistor R_L placed in parallel. The actual magnitude of the standard deviation of the vibrational force applied in the three cases is $\sigma = 3 \times 10^{-4}$ N, 6×10^{-4} N, 12×10^{-4} N. The load resistance is $R = R_L = 100$ MΩ and the piezo capacitance $C = 112nF$. The effective mass is $m = 0.0155$ kg. The damping constant is $\gamma = 0.016$ Hz.

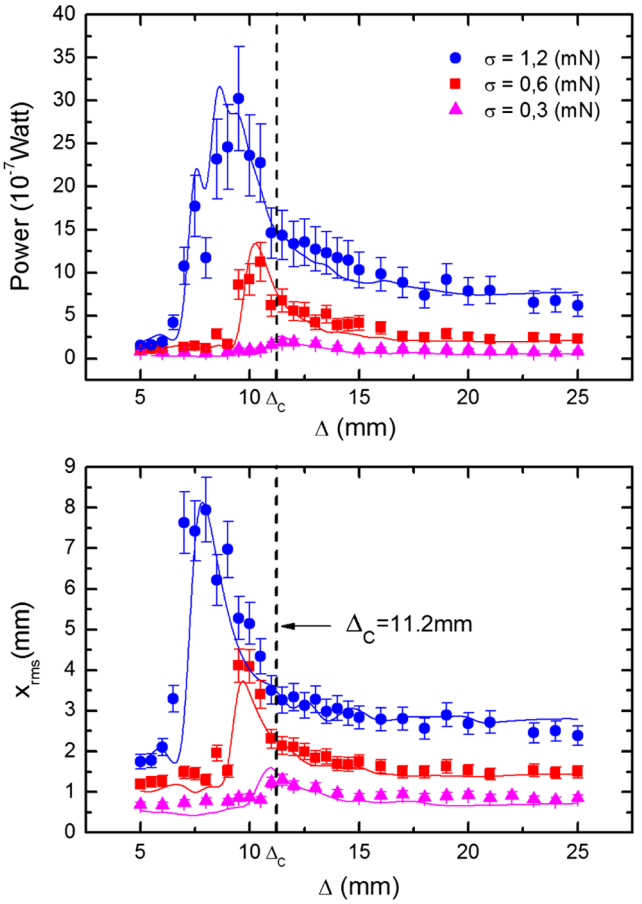

FIG. 2 (color online). Piezoelectric oscillator mean electric power (upper panel) and position $x_{\rm rms}$ as a function of Δ for three different values of the noise standard deviation σ. The symbols correspond to experimental values measured from the apparatus in Fig. 1. The continuous curves have been obtained from the numerical solution of the stochastic differential equation (1). Both in the experiment and in the numerical solution, the stochastic force has the same statistical properties with correlation time $\tau = 0.1$ s. Every data point is obtained from averaging the rms values of ten time series sampled at a frequency of 1 kHz for 200 s. The rms is computed after zero averaging the time series. The expected relative error in the numerical solution is within 10%.

measuring the voltage drop V over a resistive load R_L [7], under the influence of a random vibration with Gaussian distribution (with zero mean and standard deviation σ) and exponential autocorrelation function (with correlation time τ). In Fig. 2 (upper panel), we show the average electrical power $\langle V^2 \rangle / R_L$ as a function of Δ for three different values of the noise standard deviation σ. In all the cases, the power increases rapidly from the linear case (large Δ) up to a maximum value and then decreases when the magnets become closer and closer. A qualitatively similar behavior is observed (Fig. 2, lower panel) if we plot the pendulum rms position $x_{\rm rms}$, as a function of Δ.

In order to quantitatively account for the experiments, we developed a dynamical description of the inverted pendulum based on the following equation of motion:

$$m\ddot{x} = \frac{dU(x)}{dx} - \gamma\dot{x} - K_v V(t) + \sigma\xi(t). \qquad (1)$$

The first term on the right-hand side accounts for the conservative force, where $U(x)$ is the potential energy of the pendulum [13] shown in Fig. 3.

$$U(x) = Kx^2 + (ax^2 + b\Delta^2)^{-3/2} + c\Delta^2, \qquad (2)$$

with K, a, b, and c representing constants related to the physical parameters of the pendulum [14,15] (see Fig. 1): $K = K_{\rm eff}/2$ with $K_{\rm eff}$ effective elastic constant; $a = d^2(\mu_0 M^2/2\pi d)^{-2/3}$ with μ_0 the permeability constant, $M = 0.051$ A m^2, the effective magnetic moment, and $d = 2.97$ a geometrical parameter related to the distance between the measurement point and the pendulum length; $b = a/d^2$; and $c = K/d^2$.

The second term on the right-hand side of (1) $-\gamma\dot{x}$ accounts for the energy dissipation due to the bending, and $-K_v V(t)$ accounts for energy transferred to the electric

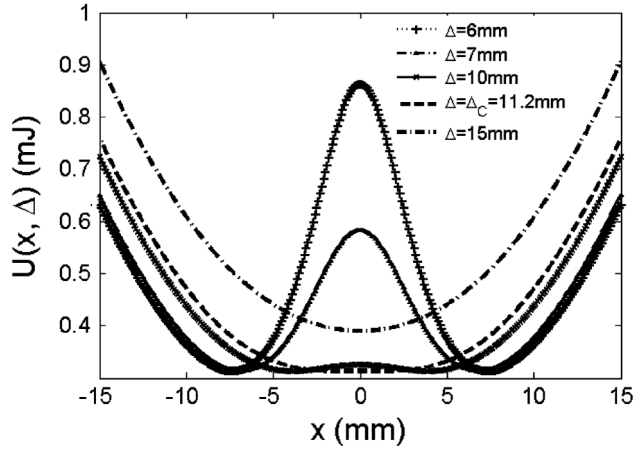

FIG. 3. Inverted pendulum potential function $U(x)$. Five different plots of the potential function (2) corresponding to five different values of the parameter Δ, representing the distance between the external magnet and the tip magnet (see Fig. 1) are shown (vertical scale in J). On decreasing Δ the potential changes from monostable to bistable.

load R_L with coupling equation:

$$\dot{V}(t) = K_c\dot{x} - \frac{V(t)}{R_L C}. \tag{3}$$

C and K_c are, respectively, the capacitance and the coupling constant of the piezoelectric sample. Finally, $\sigma\xi(t)$ accounts for the vibration force that drives the pendulum. $\xi(t)$ represents a stochastic process with the same statistical properties of the magnetic excitation. In Fig. 2, we plot with a continuous line the computed power $\langle V^2\rangle/R_L$ (upper panel) and the rms value of $x(t)$ (lower panel) as obtained by the numerical solution of the equation of motion. All the parameters have been measured from the experimental apparatus and introduced into the equation. As it is apparent, the agreement between the experimental data and the model is rather good. In Fig. 2, we can easily identify three different regimes: (1) Large Δ, i.e., $\Delta \gg \Delta_c = \alpha/\sqrt{b}$ with $\alpha = (3a/2K)^{1/5}$. The dynamics is characterized by quasilinear oscillations around the single minimum located at zero displacement, in correspondence with the vertical position of the pendulum. This condition accounts for the usual performances of a linear piezoelectric generator. (2) Small Δ ($\Delta \ll \Delta_c$), the potential energy is bistable with a very pronounced barrier between the two wells. In this condition and for a given amount of noise, the pendulum swing is almost exclusively confined within one well and the dynamics is characterized once again by quasilinear oscillations around the minimum of the confining well. (3) In between there is a range of distances Δ where the x_{rms} (and the V_{rms} as well) reaches a maximum value. In this condition the pendulum dynamics is highly nonlinear and the swing reaches its largest amplitude with noise assisted jumps between the two wells. As it is well evident in Fig. 2, the maximum values of the output power exceeds by a factor that ranges between 4 and 6 the value obtainable when the magnet is far away. This indicates a potential gain for power harvesting between 400% and 600% compared to the standard linear oscillators.

Two other important features are apparent: (a) the maximum position shifts toward larger Δ when the noise intensity increases. (b) In the low Δ regime, the rms reaches a plateau that is smaller than the plateau reached by the rms in the large Δ regime. Both features can be explained as follows. When $\Delta \gg \Delta_c$, the potential $U(x)$ shows a single minimum with librational frequency given by $\omega_0^2 = U''(0)/m = (2k - 3ab^{-5/2}/\Delta^5)/m$. The x_{rms} value here can be estimated in the linear oscillator approximation [16] as proportional to σ/ω_0. On decreasing Δ, ω_0 decreases and thus the x_{rms} value increases. When $\Delta = \Delta_c$ the potential develops two distinct minima located at $x_\pm = \pm((\alpha^2 - b\Delta^2)/a)^{1/2}$.

The pendulum swings now between the two minima and the rms increases proportional to $x_\pm$. With decreasing Δ, the potential barrier height ΔU grows proportional to Δ^{-3} and becomes so large that the jump probability becomes negligible. The pendulum swing is thus permanently confined within one well. Such a trapping condition happens at smaller values of Δ (i.e., larger barrier) for larger noise. This explains the observed shift of the maximum position toward smaller Δ as observed in (a). Inside one well the dynamics is almost linear with small oscillations around the potential local minima (x_+ or x_-) and $x_{\mathrm{rms}} \propto \sigma/\omega_\pm$ with $\omega_\pm = U''(x_\pm)/m$. Being $\omega_\pm > \omega_0$ it follows $\mathrm{rms}_{\Delta\to 0} < \mathrm{rms}_{\Delta\to\infty}$, as observed in (b). The increase in the rms value observed for the inverted pendulum is not a peculiar feature of this specific system or potential. Instead, it appears to be quite a general feature of bistable dynamical systems. To support this statement, we focussed our attention on the dynamics of the so-called Duffing oscillator [17], extensively studied in the presence of noise both in the classical [18] and in the quantum domain [19]. The potential $U_q(x) = -a/2x^2 + b/4x^4$ is bistable when $a > 0$ with $x_\pm = \pm\sqrt{a/b}$ and $\Delta U_q = a^2/4b$. The equation of motion,

$$m\ddot{x} = \frac{dU_q(x)}{dx} - \gamma\dot{x} + \sigma_q\xi(t), \tag{4}$$

is in analogy with the pendulum case. The role of Δ is played here by the parameter a. The behavior of x_{rms} is qualitatively similar to the one shown by the pendulum, i.e., three distinct regimes can be identified: (1) $a \ll 0$. The potential is monostable and the dynamics is characterized by quasilinear oscillations around the minimum located at $x = 0$. (2) $a \gg 0$. The potential is bistable with a very pronounced barrier between the two wells. The dynamics is mainly trapped inside one minimum. (3) In between there is a range of values where x_{rms} reaches a maximum and the dynamics is characterized by frequent jumps between the two wells.

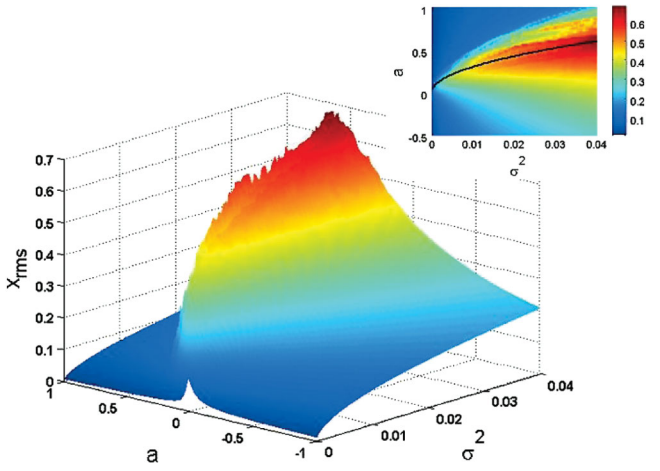

FIG. 4 (color). Root mean squared (rms) values of the Duffing oscillator position x_{rms} as a function of a and the noise variance σ^2. The values plotted here have been obtained from the numerical solution of (4). rms is computed after zero averaging the $x(t)$. Inset: contour plot of x_{rms}. The continuous line represents the theoretical prediction for the maximum: i.e. x_{rms} has a maximum when $a = \sqrt{b\sigma^2\tau}$. The expected relative error in the numerical solution is within 10%.

In Fig. 4, we present the x_{rms} as a function of a and the noise variance σ^2. The contour plot in the figure inset shows the evolution of the maximum x_{rms}. The solid line is a theoretical prediction obtained with the following argument. The rms evolution in regime (3) can be roughly modeled as governed by to two main contributions: (i) the raising, mainly due to the growth of the separation between the two minima at $x_{\pm}$; (ii) the drop, mainly due to the decrease in the jump probability measured by the crossing probability, proportional [20] to $\exp(-\Delta U_q/\sigma^2\tau)$, caused by the increase of the potential barrier height ΔU_q. For the sake of identifying the dependence of the maximum position, we computed the root of the equation:

$$\frac{dx_{\mathrm{rms}}}{da} = \frac{d}{da}(x_+ e^{-(\Delta U_q/\sigma^2\tau)}) = 0 \qquad (5)$$

obtaining that x_{rms} reaches a maximum when $a = a_{\mathrm{max}} = \sqrt{b\sigma^2\tau}$ for a given noise intensity.

Finally, we notice that the dynamical features discussed here are not limited to the sole piezoelectric energy conversion but can be applied also to other principles, e.g., capacitive and inductive. They can be applied also to micro [21] and nanomechanical resonators [8,22] where noise driven dynamics are considered as a promising option [23]. In any case no conversion of equilibrium thermal energy is implied.

Useful discussions with P. Amico, I. Neri, and F. Marchesoni are gratefully acknowledged.

*Present address: Stokes Institute, University of Limerick ER02-009, Limerick, Ireland
†luca.gammaitoni@pg.infn.it

[1] J. A. Paradiso and T. Starner, IEEE Pervasive Computing **4**, 18 (2005).
[2] S. Roundy, P. K. Wright, and J. M. Rabaey, *Energy Scavenging for Wireless Sensor Networks* (Kluwer Academic Publishers, Boston, 2003).
[3] R. Byrne and D. Diamond, Nature Mater. **5**, 421 (2006).
[4] S. Meninger *et al.*, IEEE Transactions on Very Large Scale Integration (VLSI) Systems **9**, 64 (2001).
[5] P. D. Mitcheson *et al.*, J. Microelectromech. Syst. **13**, 429 (2004).
[6] S. Roundy and P. K. Wright, Smart Materials and Structures **13**, 1131 (2004).
[7] Y. C. Shu and I. C. Lien, Smart Materials and Structures **15**, 1499 (2006).
[8] Z. L. Wang and J. Song, Science **312**, 242 (2006).
[9] T. von Buren and G. Troster, Sens. Actuators A, Phys. **135**, 765 (2007).
[10] S. R. Anton and H. A. Sodano, Smart Materials and Structures **16**, R1 (2007).
[11] S. Wang *et al.*, Appl. Phys. Lett. **90**, 113506 (2007); S. Roundy, J. Intell. Mater. Syst. Struct. **16**, 809 (2005); S. P. Beeby, M. J. Tudor, and N. M. White, Meas. Sci. Technol. **17**, R175 (2006).
[12] The technology based on the exploitation of bistable oscillators is called "wisepower" technology and patented by Wisepower srl.
[13] Y. Kraftmakher, Eur. J. Phys. **28**, 409 (2007).
[14] E. Lefeuvre *et al.*, Sens. Actuators A, Phys. **126**, 405 (2006).
[15] Y. C. Shu and I. C. Lien, J. Micromech. Microeng. **16**, 2429 (2006).
[16] M. Gitterman, Physica A (Amsterdam) **352**, 309 (2005).
[17] G. Duffing, *Duffing, Erzwungene Schwingungen bei Veränderlicher Eigenfrequenz and Ihre Technische Bedeutung* (F. Vieweg u. Sohn, Braunschweig, 1918).
[18] M. Rahman, Phys. Rev. E **53**, 6547 (1996).
[19] T. Dittrich, B. Oelshlagel, and P. Hanggi, Europhys. Lett. **22**, 5 (1993).
[20] P. Hanggi, P. Talkner, and M. Borkovec, Rev. Mod. Phys. **62**, 251 (1990).
[21] H. B. Fang *et al.*, Microelectron. J. **37**, 1280 (2006).
[22] J. S. Aldridge and A. N. Cleland, Phys. Rev. Lett. **94**, 156403 (2005).
[23] L. Gammaitoni and A. R. Bulsara, Phys. Rev. Lett. **88**, 230601 (2002); R. Almog, S. Zaitsev, O. Shtempluck, and E. Buks, Phys. Rev. Lett. **98**, 078103 (2007).